Light distribution close to focus in biaxially birefringent media

Sjoerd Stallinga

Philips Research Laboratories, Professor Holstlaan 4, 5656 AA Eindhoven, The Netherlands

Received October 15, 2003; revised manuscript received February 18, 2004; accepted April 2, 2004

The effect of focusing into a biaxially birefringent medium on the light distribution in the focal region of a high-NA optical system is investigated with the Debye approach to vectorial diffraction theory. Attention is limited to media with small birefringence. The electric field in the focal region is the sum of the field of the two polarization eigenmodes of the biaxially birefringent medium. Both modes are generally astigmatically aberrated, are defocused with respect to each other, and have a polarization field that is nonuniform over the pupil. The diffraction integrals are calculated numerically on the basis of an expansion of the field close to focus in terms of partial waves. © 2004 Optical Society of America

OCIS codes: 260.1440, 260.1960, 210.4770, 180.1790.

1. INTRODUCTION

The light distribution close to focus in various circumstances is relevant to the imaging properties of scanning microscopes and to the readout of optical disks. Focusing through or into a birefringent layer results in blurring of the focal spot that deteriorates the image of a scanning microscope and the readout of significant bits from an optical disk. These birefringence effects can occur in the substrate–cover layer of optical disks as a result of mechanical stresses that are introduced into the plastic during manufacturing. As the beam is focused onto the data layer through the substrate–cover layer, birefringence in the latter layer can be particularly harmful. The aim of this paper is to study the effect on the focal spot of focusing into a biaxially birefringent medium. Such a medium has three different refractive indices associated with three mutually orthogonal axes, the principal axes. This paper generalizes the results obtained in a previous paper[1] on the effect of focusing into a uniaxially birefringent layer with principal axis parallel to the optical axis.

The focal light distribution can be studied within the framework of vectorial diffraction theory. Focusing in a single isotropic medium was originally considered by Wolf and coworkers,[2–5] and later by Mansuripur,[6–8] Kant,[9,10] and Sheppard and Török.[11] Focusing through an interface between two dielectric media was first investigated by Ling and Lee,[12] followed by a number of other authors.[13–19] A general framework for describing focusing into uniaxial and biaxial anisotropic media was developed by Stamnes and coworkers.[20–24] In Ref. 24 the formalism is applied to the paraxial limit of small NAs.

This paper deals mainly with biaxially birefringent media with small birefringence. This means that the differences between the three refractive indices are taken to be much smaller than 1. For stress-induced birefringence in the plastic substrate–cover layer of optical disks these differences are of the order of 10^{-5}–10^{-3}, which makes the approximation quite appropriate for this case. There are also many crystals for which the small-birefringence approximation is justified. For example, the short list of biaxial crystals mentioned in Ref. 25 includes gypsum, feldspar, mica, topaz, and $YAlO_3$, for which the birefringence parameters are of the order of 10^{-3} or less. The main advantage of the small-birefringence approximation is that it allows for a considerable simplification of the formalism needed to calculate the light distribution close to focus. Such a simplified formalism clarifies the physical effects governing the deformation of the focal spot by the effects of birefringence. For example, in Ref. 1 it is shown that the spot distortion is determined largely by a relative defocus of the ordinary and extraordinary polarization modes. Results that are similar in character can be obtained for the case of biaxial birefringence.

The content of this paper is as follows. The existing results in the literature based on the Debye approach are summarized in Section 2. These results are generalized to biaxially birefringent media in Section 3. Numerical results are discussed in Section 4. The paper concludes with a summary of the main results in Section 5.

2. DEBYE APPROACH

A. Light Distribution Close to Focus

We consider a collimated beam of light of wavelength λ propagating in the z direction that is focused by a lens into a biaxially birefringent medium with refractive indices that deviate slightly from an average refractive index n. The cone of light converging to focus has a top angle 2β making $\mathrm{NA} = n \sin\beta$. The distance between the interface and the focal point is d. In the Debye approach the electromagnetic field close to the focal point is expressed as a superposition of plane waves. Each of these plane waves corresponds to a point on the reference sphere of radius R touching the exit pupil, as shown in Fig. 1. The propagation direction of the plane wave is along the line between the corresponding point on the reference sphere and the (geometrical) focal point of the lens. Clearly, plane waves with wave vectors $\mathbf{k} = nk\hat{k}$, with $k = 2\pi/\lambda$, and

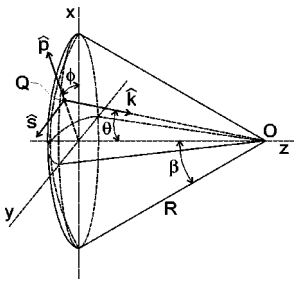

Fig. 1. Reference sphere centered at the focal point O. The radius is R and the maximum polar angle, defined by the aperture of the lens, is β. A point Q on the reference sphere corresponds to a plane wave contributing to the field at focus. The unit vector $\hat{k}$ along the wave vector is parametrized by the polar angle θ and the azimuthal angle ϕ, where θ is always smaller than β. The electric field is a linear combination of the polarization vectors $\hat{p}$ and $\hat{s}$.

$$\hat{k} = (\sin\theta\cos\phi,\ \sin\theta\sin\phi,\ \cos\theta), \tag{1}$$

contribute to focus if the polar angle $\theta \leqslant \beta$. This sharp cutoff in the angular spectrum of plane waves is the basic assumption of the Debye approach and is valid provided the Fresnel number N is much larger than 1. The Fresnel number is typically the ratio of the pupil radius $a = R\sin\beta$ and the diffraction length λ/NA. The pupil radius is taken to be of the order of 1 mm and the diffraction length is of the order of 1 μm for visible light and moderate to high NA, giving a Fresnel number of the order of 10^3. It follows that the Debye approach may be safely applied. Even for small NA values, well within the paraxial regime, the Fresnel number is still sufficiently large that the Debye approach can be applied. The lower limit for NA is $\approx 10^{-2}$ for visible light and a fixed pupil radius of the order of 1 mm. A more extensive discussion of the validity of the Debye aproach can be found in the texts by Stamnes.[26,27]

It is often convenient to map this part of the reference sphere to the unit circle. The position vector of a point in the unit circle

$$\boldsymbol{\rho} = (\rho\cos\phi,\ \rho\sin\phi) \tag{2}$$

is associated with a direction parametrized by θ and ϕ for the following definition of the radial pupil coordinate ρ:

$$\rho = \sin\theta/\sin\beta. \tag{3}$$

It follows that ρ is a measure of the distance between the optical axis and the point on the reference sphere associated with the plane wave with polar angle θ.

Associated with each plane wave are the p- and s-polarization vectors (see Fig. 1):

$$\hat{p} = (\cos\theta\cos\phi,\ \cos\theta\sin\phi,\ -\sin\theta), \tag{4}$$

$$\hat{s} = (-\sin\phi,\ \cos\phi,\ 0). \tag{5}$$

The vectors $\hat{p}$, $\hat{s}$, and $\hat{k}$ make an orthonormal set with $\hat{p} \times \hat{s} = \hat{k}$. Both the electric and magnetic fields in the far field $R \gg \lambda$ are in the plane spanned by $\hat{p}$ and $\hat{s}$.

The goal of our work is to calculate the electromagnetic field in the proximity of the geometrical focus. This point is taken to be the center of our coordinate frame. A point $\mathbf{r}_p$ in the proximity of focus can be parameterized in spherical coordinates as

$$\mathbf{r}_p = (r_p\sin\theta_p\cos\phi_p,\ r_p\sin\theta_p\sin\phi_p,\ r_p\cos\theta_p). \tag{6}$$

A different parametrization is in (normalized) cylindrical coordinates as

$$\mathbf{r}_p = \left(\frac{\lambda}{\mathrm{NA}}v\cos\phi_p,\ \frac{\lambda}{\mathrm{NA}}v\sin\phi_p,\ \frac{n\lambda}{\mathrm{NA}^2}u\right), \tag{7}$$

where u and v are the normalized axial and radial coordinates, respectively (see Fig. 2).

The literature on vectorial diffraction based on the Debye approach can be summarized by the following formula for the components of the electric field $\mathbf{E}$ at a point $\mathbf{r}_p$ in the proximity of focus:

$$E_\alpha(\mathbf{r}_p) = \frac{E_0\pi N}{i}\sum_{j=1,2}F_{\alpha j}(\mathbf{r}_p)A_j, \tag{8}$$

for $\alpha = x, y, z$. Here E_0 is the amplitude in the entrance pupil; A_1 and A_2 are the x and y components of the polarization vector in the entrance pupil, respectively; $N = R\sin^2\beta/\lambda$ is the Fresnel number; and the functions $F_{\alpha j}$ are defined by the integrals over the reference sphere (the angular range $0 \leqslant \theta \leqslant \beta$, $0 \leqslant \phi \leqslant 2\pi$) as

$$\begin{aligned} F_{\alpha j}(\mathbf{r}_p) &= \frac{1}{\pi\sin^2\beta}\int_R \mathrm{d}\Omega\cos\theta\sum_{l=1,2}\hat{v}_{l\alpha}J_{lj}\exp(i\Phi) \\ &= \frac{1}{\pi}\int_R \mathrm{d}^2\rho\sum_{l=1,2}\hat{v}_{l\alpha}J_{lj}\exp(i\Phi), \end{aligned} \tag{9}$$

where $\mathrm{d}\Omega = \sin\theta\,\mathrm{d}\theta\mathrm{d}\phi$, Φ is the phase, $\hat{v}_l$ are the polarization vectors, and J is a 2×2 matrix, the Jones matrix. All quantities depend on the pupil coordinates ρ and ϕ, or equivalently, θ and ϕ. The polarization vectors are a linear combination of $\hat{p}$ and $\hat{s}$:

$$\begin{aligned} \hat{v}_1 &= \cos\phi\hat{p} - \sin\phi\hat{s} \\ &= (\cos\theta\cos^2\phi + \sin^2\phi,\ -(1 \\ &\quad - \cos\theta)\sin\phi\cos\phi,\ -\sin\theta\cos\phi), \end{aligned} \tag{10}$$

$$\begin{aligned} \hat{v}_2 &= \sin\phi\hat{p} + \cos\phi\hat{s} \\ &= (-(1 - \cos\theta)\sin\phi\cos\phi,\ \cos^2\phi \\ &\quad + \cos\theta\sin^2\phi,\ -\sin\theta\sin\phi), \end{aligned} \tag{11}$$

and do not depend on the image position $\mathbf{r}_p$. The Jones matrix does not depend on the image position either. The phase is the only quantity that depends on the image position $\mathbf{r}_p$, and can be written as

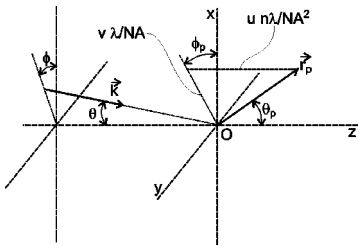

Fig. 2. Parametrization of the wavevector $\mathbf{k}$ by the polar and azimuthal angles θ and ϕ, respectively, and of the position vector $\mathbf{r}_p$ by spherical coordinates r_p, θ_p, and ϕ_p and by dimensionless cylindrical coordinates u, v, and ϕ_p.

$$\begin{aligned}\Phi &= \mathbf{k}\cdot\mathbf{r}_p \\ &= nkr_p(\sin\theta\sin\theta_p\cos(\phi-\phi_p)+\cos\theta\cos\theta_p) \\ &= 2\pi v\rho\cos(\phi-\phi_p)-\frac{2\pi u\rho^2}{1+(1-\rho^2\sin^2\beta)^{1/2}} \\ &\quad +\frac{2\pi u}{\sin^2\beta}. \end{aligned} \tag{12}$$

The second line gives the expression in spherical coordinates, the third in dimensionless cylindrical coordinates. The third term of the third line, a phase term not depending on the pupil coordinates, is usually left out. It is noted that the magnetic field can be expressed similarly to the electric field, but with polarization vectors $\hat{w}_l$ that are found from the electric polarization vectors $\hat{v}_l$ by the substitutions $\hat{p}\rightarrow\hat{s}$ and $\hat{s}\rightarrow-\hat{p}$.

B. Jones Matrix in Known Cases

The Jones matrix can take different forms. In case the amplitude and phase are constant over the exit pupil of the focusing lens, it is equal to the unit matrix

$$J=\begin{bmatrix}1 & 0\\ 0 & 1\end{bmatrix}. \tag{13}$$

When the amplitude and phase vary over the exit pupil the Jones matrix is given by

$$J=B\exp(iW)\begin{bmatrix}1 & 0\\ 0 & 1\end{bmatrix}, \tag{14}$$

with B and W (which are functions of $\boldsymbol{\rho}$) the apodization and aberration function, respectively. The lens is often considered to be aplanatic. Assuming a uniform amplitude in the entrance pupil, the apodization function is then given by

$$B=\frac{1}{\sqrt{\cos\theta}}=(1-\rho^2\sin^2\beta)^{-1/4}. \tag{15}$$

This is the original case considered by Richards and Wolf.[3] A more complicated case is that of focusing through an interface between a medium with refractive index n_1 and a medium with $n_2=n$. It is often the case that the spherical aberration introduced in this manner is corrected for by the lens. For example, in the practice of optical disk readout the scanning objective lens is designed such that the spherical aberration induced by a substrate–cover layer of nominal thickness is compensated for, leading to a diffraction-limited scanning spot. Residual spherical aberration is then related to a deviation of the thickness from the nominal thickness or to deviations in the refractive index from the assumed nominal value of the plastic. For such corrected systems the phase factor corresponding to spherical aberration can be left out. Furthermore, the distortion of the focal spot by spherical aberration can overshadow the more subtle effects of the interface itself, or of the birefringence of the medium. As this paper deals with the latter effect, the spherical aberation is ignored in our treatment. This leads to a Jones matrix:

$$\begin{aligned}J &= R(\phi)\begin{bmatrix}t_p & 0\\ 0 & t_s\end{bmatrix}R(-\phi) \\ &= \begin{bmatrix}t_p\cos^2\phi+t_s\sin^2\phi & (t_p-t_s)\sin\phi\cos\phi\\ (t_p-t_s)\sin\phi\cos\phi & t_s\cos^2\phi+t_p\sin^2\phi\end{bmatrix}.\end{aligned} \tag{16}$$

Here $R(\phi)$ is the rotation matrix,

$$R(\phi)=\begin{bmatrix}\cos\phi & -\sin\phi\\ \sin\phi & \cos\phi\end{bmatrix}, \tag{17}$$

and t_p and t_s are the p and s Fresnel coefficients,

$$t_p=\frac{2n_1\cos\theta_1}{n_1\cos\theta_2+n_2\cos\theta_1}, \tag{18}$$

$$t_s=\frac{2n_1\cos\theta_1}{n_1\cos\theta_1+n_2\cos\theta_2}, \tag{19}$$

where θ_1 and $\theta_2=\theta$ are the angles of incidence in medium 1 and 2, respectively, related by Snell's law. The matrix $R(-\phi)JR(\phi)$ is the Jones matrix on the basis formed by the p- and s-polarization vectors, i.e., it relates the complex p and s amplitudes on the exit side to the complex p and s amplitudes on the entrance side. The apodization factor related to the aplanatic condition is now $B=1/\sqrt{\cos\theta_1}$. The case of a single interface can be generalized to the case of multilayer interference stacks, which may include evanescent wave coupling through layers of subwavelength thickness.

A somewhat more complicated case is that of a uniaxially birefringent medium with its principal axis along the optical axis of the system (the z axis). This is the case of axial birefringence treated in Ref. 1. The conventional designation "optic axis" for the principal or symmetry axis of the uniaxial medium is avoided to prevent confusion with the term "optical axis" (the line through the center of the pupil and the geometrical focal point). Furthermore, similar nomenclature is used for uniaxial and biaxial media. For biaxial media the three principal axes (the axes that define a frame in which the dielectric tensor is diagonal) do not coincide with the optic axes (the axes along which the two orthogonal polarization modes have the same refractive index).

The ordinary and extraordinary refractive indices are n and $n+\Delta n$, respectively, and the birefringence Δn is assumed to be small compared to 1. The ordinary mode corresponds to the field component that is tangentially or s polarized in the exit pupil of the lens, whereas the extraordinary mode corresponds to the field that is radially or p polarized in the exit pupil of the lens. This implies that the Jones matrix on the basis of the p and s polarization vectors is diagonal. The diagonal terms of this matrix depend on the p and s aberration functions, which are given by

$$W_p=W+\Delta W=W+\frac{kd\Delta n\sin^2\theta'}{\cos\theta'}, \tag{20}$$

$$W_s=W. \tag{21}$$

Here W is the classical isotropic aberration function, d is the distance between the entrance interface and the geo-

metrical focus, and θ', the polar angle of the wave vector inside the medium, is related to the dimensionless pupil coordinate ρ by $\sin\theta' = \rho \mathrm{NA}/n$.

When focusing into the birefringent layer is considered, the effect of the interface must also be taken into account. This may be done with an interface matrix that gives the coupling between the s and p amplitudes of the field in the isotropic media in front of the birefringent medium and the e and o amplitudes of the field inside the medium. Such interface matrices can be considerably simplified in the limit of small birefringence.[25] Then the interface coupling may be approximated by neglecting the birefringence of the medium. The effect of birefringence then appears only in the phases accumulated by the polarization eigenmodes as the wave traverses the medium to the focal point; the effect of the birefringence on the amplitudes of the polarization eigenmodes is neglected. It turns out[1] that for focusing into the birefringent medium the overall Jones matrix is $J_{\mathrm{bir}} J_{\mathrm{en}}$, where J_{en} is the interface Jones matrix as defined in Eq. (16) and J_{bir} is the birefringence Jones matrix, defined by

$$J_{\mathrm{bir}} = R(\phi)\begin{bmatrix}\exp(iW_p) & 0\\ 0 & \exp(iW_s)\end{bmatrix}R(-\phi)$$
$$= \begin{bmatrix}\exp(iW_p)\cos^2\phi + \exp(iW_s)\sin^2\phi & [\exp(iW_p) - \exp(iW_s)]\sin\phi\cos\phi\\ [\exp(iW_p) - \exp(iW_s)]\sin\phi\cos\phi & \exp(iW_s)\cos^2\phi + \exp(iW_p)\sin^2\phi\end{bmatrix}. \quad (22)$$

For focusing through a birefringent slab the overall Jones matrix is $J_{\mathrm{ex}} J_{\mathrm{bir}} J_{\mathrm{en}}$, where J_{ex} is the interface matrix corresponding to the exit side of the slab. The factorization of Jones matrices for focusing through the birefringent slab is accurate only if multiple reflections can be neglected.

C. Electromagnetic Energy Density

The energy density of the electric field is $U = 1/2\varepsilon_0\varepsilon_{\alpha\beta}E_\alpha E_\beta^*$, where the dielectric tensor $\varepsilon_{\alpha\beta}$ is assumed to be real. This may be approximated by the sum over the energy densities of the x, y, and z components of the electric field, where the energy density of the α component of the electric field is $U_\alpha = 1/2\varepsilon_0\bar{n}^2|E_\alpha|^2$, because the difference between the refractive indices is assumed to be much smaller than the average refractive index $\bar{n}$. By introducing the scaling factor

$$U_0 = \tfrac{1}{2}\varepsilon_0\bar{n}^2\pi^2 E_0{}^2 N^2, \quad (23)$$

it is found that

$$U_\alpha = U_0\sum_{j,l=1,2} F_{\alpha j}F_{\alpha l}^* A_j A_l^*$$
$$= U_0\sum_{\mu=0,3} I_{\alpha\mu}M_\mu, \quad (24)$$

with the quantities

$$I_{\alpha 0} = \tfrac{1}{2}(|F_{\alpha 1}|^2 + |F_{\alpha 2}|^2), \quad (25)$$

$$I_{\alpha 1} = \tfrac{1}{2}(|F_{\alpha 1}|^2 - |F_{\alpha 2}|^2), \quad (26)$$

$$I_{\alpha 2} = \mathrm{Re}\{F_{\alpha 1}F_{\alpha 2}^*\}, \quad (27)$$

$$I_{\alpha 3} = \mathrm{Im}\{F_{\alpha 1}F_{\alpha 2}^*\}, \quad (28)$$

and the Stokes parameters M_j, which describe the state of polarization in the entrance pupil:

$$M_0 = |A_1|^2 + |A_2|^2 = 1, \quad (29)$$

$$M_1 = |A_1|^2 - |A_2|^2 = \cos 2\epsilon\cos 2\xi, \quad (30)$$

$$M_2 = 2\,\mathrm{Re}\{A_1^* A_2\} = \cos 2\epsilon\sin 2\xi, \quad (31)$$

$$M_3 = 2\,\mathrm{Im}\{A_1^* A_2\} = \sin 2\epsilon. \quad (32)$$

Here ϵ is the ellipticity angle and ξ is the angle between the long axis of the polarization ellipse and the x axis. Eq. (24) is valid for arbitrary states of polarization in the entrance pupil. Finally, it is noted that expressions for the magnetic energy density $1/2\mu_0\mathbf{H}^2$ and for the Poynting vector $\mathbf{S} = \mathrm{Re}\{\mathbf{E}\times\mathbf{H}^*\}$ can be derived along similar lines.

3. JONES MATRIX IN THE CASE OF BIAXIAL BIREFRINGENCE

A. General Expression for the Jones Matrix

In this section we consider the generalization of the Jones matrix for the case of axial birefringence to the case of biaxial birefringence. The biaxially birefringent layer has refractive indices n_1, n_2, and n_3, and principal axes

$$\hat{a}_1 = (\cos\gamma, \sin\gamma, 0), \quad (33)$$

$$\hat{a}_2 = (-\sin\gamma, \cos\gamma, 0), \quad (34)$$

$$\hat{a}_3 = (0, 0, 1); \quad (35)$$

i.e., one of the principal axes is taken parallel to the optical axis. The three refractive indices are parameterized as

$$n_1 = \bar{n}/(1 - \Delta n_\parallel/\bar{n})^{1/2}, \quad (36)$$

$$n_2 = \bar{n}/(1 + \Delta n_\parallel/\bar{n})^{1/2}, \quad (37)$$

$$n_3 = \bar{n}/(1 - 2\Delta n_\perp/\bar{n})^{1/2}, \quad (38)$$

where $\bar{n}$ is an average refractive index, $\Delta n_\parallel$ is the lateral birefringence, and $\Delta n_\perp$ is the axial birefringence. This parametrization is somewhat arbitrary and is motivated primarily by future convenience. In the limit of small birefringence these expressions may be approximated by

$$n_1 = \bar{n} + \Delta n_\parallel/2, \quad (39)$$

$$n_2 = \bar{n} - \Delta n_\parallel/2, \quad (40)$$

$$n_3 = \bar{n} + \Delta n_\perp. \quad (41)$$

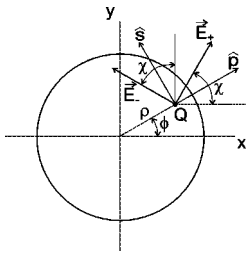

Fig. 3. Polarization fields of the two eigenmodes $\mathbf{E}_+$ and $\mathbf{E}_-$ make an angle $\chi - \phi$ with $\hat{p}$ and $\hat{s}$, respectively. The angle between the eigenpolarizations and the Cartesian x and y axes is therefore χ. This angle χ can vary with the pupil point Q.

There are two polarization eigenmodes with aberration functions W_+ and W_-. They correspond to two orthogonal polarization fields that are a linear sum of the p- and s-polarization fields. The angle between the +mode polarization vector and $\hat{p}$ (which is equal to the angle between the −mode polarization vector and $\hat{s}$) is $\chi - \phi$ (see Fig. 3). With $R(-\phi)JR(\phi)$ as the Jones matrix on the basis formed by the p- and s-polarization vectors, the Jones matrix J then follows as

$$J = R(\chi)\begin{bmatrix}\exp(iW_+) & 0\\ 0 & \exp(iW_-)\end{bmatrix}R(-\chi)$$
$$= \begin{bmatrix}\exp(iW_+)\cos^2\chi + \exp(iW_-)\sin^2\chi & [\exp(iW_+) - \exp(iW_-)]\sin\chi\cos\chi\\ [\exp(iW_+) - \exp(iW_-)]\sin\chi\cos\chi & \exp(iW_+)\sin^2\chi + \exp(iW_-)\cos^2\chi\end{bmatrix}. \quad (42)$$

The aberration functions turn out to be

$$W_\pm = \frac{kd}{2\cos\theta'}[a \pm (b^2 + c^2)^{1/2}], \quad (43)$$

and the angle χ follows from

$$\cos(2\chi - 2\phi) = b/(b^2 + c^2)^{1/2}, \quad (44)$$

$$\sin(2\chi - 2\phi) = c/(b^2 + c^2)^{1/2}, \quad (45)$$

where the quantities a, b, and c are defined as

$$a = \Delta n_\perp \sin^2\theta' - \tfrac{1}{2}\Delta n_\parallel \sin^2\theta'\cos(2\gamma - 2\phi), \quad (46)$$

$$b = \Delta n_\perp \sin^2\theta' + \tfrac{1}{2}\Delta n_\parallel(1 + \cos^2\theta')\cos(2\gamma - 2\phi), \quad (47)$$

$$c = \Delta n_\parallel \cos\theta' \sin(2\gamma - 2\phi), \quad (48)$$

and where θ' is given by $\sin\theta' = \rho\mathrm{NA}/\bar{n}$. A formal derivation of these results is presented in Subsection 3.B. It is remarked that the overall Jones matrix must also take into account the interfaces between the birefringent layer and the isotropic entrance medium. In the limit of small birefringence this interface can be described by the isotropic Fresnel coefficients, just as discussed in Subsection 2.B for the special case of axial birefringence. The overall Jones matrix for focusing into the birefringent medium is then $J_{\mathrm{bir}}J_{\mathrm{en}}$, where J_{bir} is the birefringence Jones matrix of Eq. (42) and J_{en} is the interface Jones matrix of Eq. (16). For focusing through a birefringent slab the overall Jones matrix is $J_{\mathrm{ex}}J_{\mathrm{bir}}J_{\mathrm{en}}$, where J_{ex} is the Jones matrix of the exit surface, and where multiple reflections are neglected.

In the special case of uniaxial birefringence with principal axis along the optical axis, so-called axial birefringence ($\Delta n_\parallel = 0$), the aberration functions (taking $\Delta n_\perp > 0$) are

$$W_+ = \frac{2\pi d\Delta n_\perp \sin^2\theta'}{\lambda\cos\theta'}, \quad (49)$$

$$W_- = 0, \quad (50)$$

and the eigenpolarization angle is $\chi = \phi$, in agreement with my previous paper.[1] The two polarization eigenmodes are now the purely radially polarized field (extraordinary mode) and the purely azimuthally polarized field (ordinary mode). The difference aberration function $W_+ - W_-$ is proportional to ρ^2 for small θ', meaning that the two focal spots are relatively defocused. The spherical aberration terms of all orders that appear as well are less important. Figure 4 shows the aberration functions (with the average defocus subtracted) and polarization fields of the two eigenmodes for $\Delta n_\perp = 0.016$ (and $\Delta n_\parallel = 0$). The defocus difference between the two modes and the radial and azimuthal eigenpolarizations are clearly visible. The parameters that are used are $\bar{n} = 1.58$, NA = 0.85, $d = 100$ μm, and $\lambda = 405$ nm and pertain to the readout of so-called Blu-ray disks.[28–30] This new type of optical disk has a significantly higher storage capacity (≈25 Gbyte) than existing compact disks (CDs, 650 Mbyte) and digital versatile disks (DVDs, 4.7 Gbyte) as a result of the use of a shorter wavelength (785 nm for CD and 655 nm for DVD) and a larger NA (0.45–0.50 for CD and 0.60–0.65 for DVD).

In the special case of uniaxial birefringence with principal axis perpendicular to the optical axis—so-called lateral birefringence, ($\Delta n_\perp = -\Delta n_\parallel/2$, i.e., $n_3 = n_2$)—the aberration functions (taking $\Delta n_\parallel > 0$) are

$$W_+ = \frac{\pi d\Delta n_\parallel}{\lambda\cos\theta'}[1 - 2\sin^2\theta'\cos^2(\gamma - \phi)], \quad (51)$$

$$W_- = -\frac{\pi d\Delta n_\parallel}{\lambda\cos\theta'}. \quad (52)$$

The aberration function of the extraordinary mode contains terms $\rho^2\cos(2\gamma - 2\phi)$ and ρ^2 for small θ', meaning that this mode suffers from astigmatism and defocus. The aberration function of the ordinary mode suffers from defocus alone. The amount of defocus in the two modes is the same and can therefore be eliminated by a shift of

the image plane. The eigenpolarization angle χ is given by

$$\cos(2\chi - 2\phi) = \frac{\cos(2\gamma - 2\phi) - \sin^2\theta' \cos^2(\gamma - \phi)}{1 - \sin^2\theta' \cos^2(\gamma - \phi)}, \tag{53}$$

$$\sin(2\chi - 2\phi) = \frac{\cos\theta' \sin(2\gamma - 2\phi)}{1 - \sin^2\theta' \cos^2(\gamma - \phi)}. \tag{54}$$

For small polar angles θ' it follows that $\chi = \gamma$. For large polar angles θ', deviations occur that are of second order in θ'. Figure 5 shows the aberration functions (with the average defocus subtracted) and polarization fields for $\Delta n_\parallel = -2\Delta n_\perp = 0.016$ (and the same values for $\bar{n}$, NA, d, and λ as for the axial birefringence case). The saddle shape of the extraordinary aberration function and the near flatness of the ordinary aberration function imply that there is no defocus difference and that the extraordinary mode is astigmatically aberrated. The eigenpolarizations turn out to be indeed nearly uniformly linear.

For a general biaxial layer a crossover between the salient features of the two uniaxial cases takes place as the ratio $\Delta n_\parallel/\Delta n_\perp$ varies. The pupil point on the optical axis where $W_+ = W_-$ for $\Delta n_\parallel = 0$ splits into two points where $W_+ = W_-$ when $\Delta n_\parallel \neq 0$. These zero-retardation points in the pupil correspond to the optic axes of the biaxial medium. These two distinct optic axes of the biaxial medium are at the heart of the phenomenon of conical refraction.[31] The absence of retardation for propagation along the optic axes has been used by Goodman and Mansuripur[32] to measure the birefringence parameters. The polar angle of incidence (in the birefringent layer) θ_c is given by (take $\Delta n_\parallel > 0$ and $\Delta n_\perp > 0$)

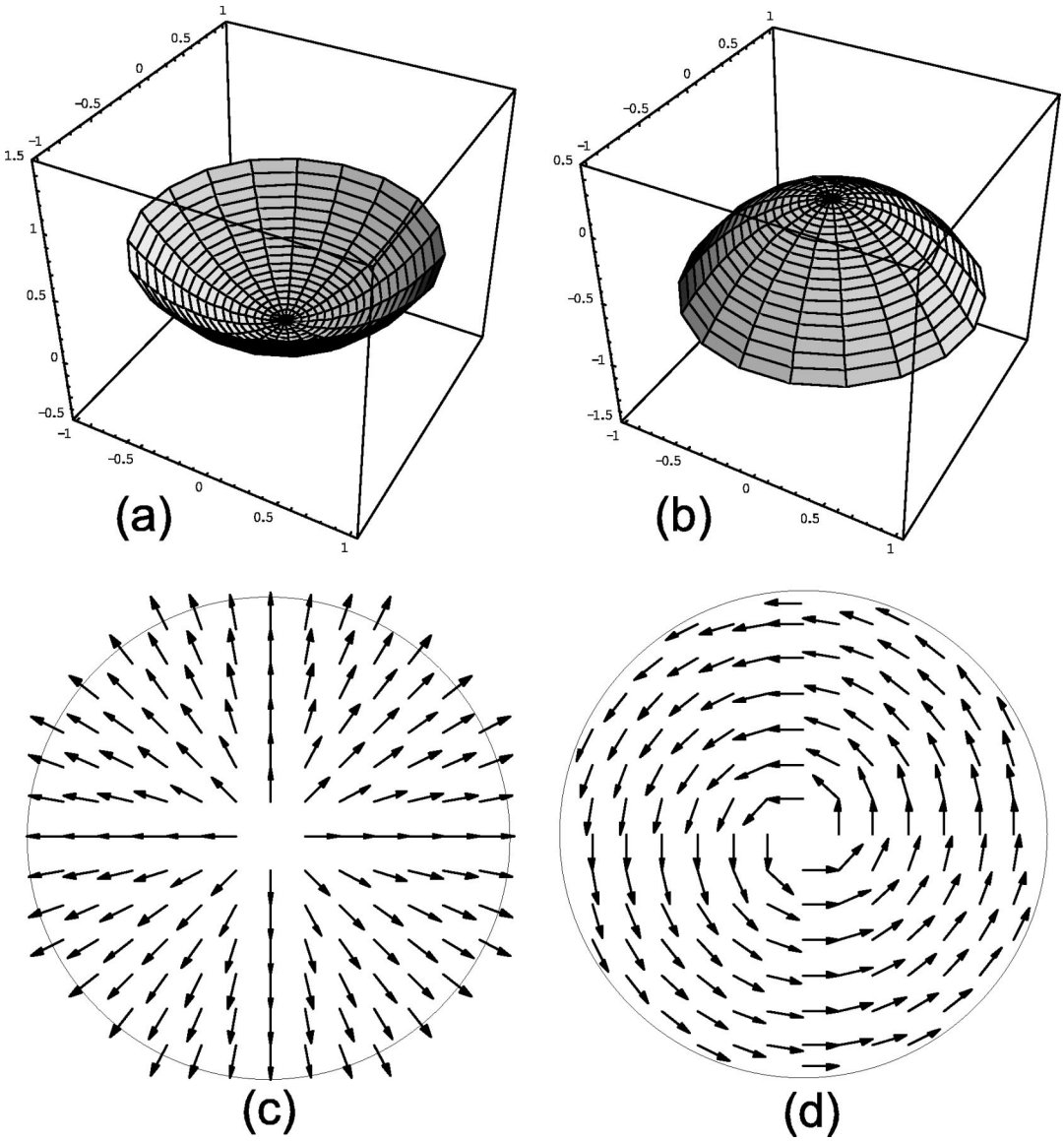

Fig. 4. Aberration functions of the (a) extraordinary and (b) ordinary modes, and polarization fields of the (c) extraordinary and (d) ordinary modes as a function of pupil coordinates for a uniaxially birefringent layer with optic axis parallel to the optical axis. The circle in (c) and (d) indicates the pupil rim. We have taken $\Delta n_\perp = 0.016$, $\Delta n_\parallel = 0$, $\bar{n} = 1.58$, NA = 0.85, $d = 100$ μm, and $\lambda = 0.405$ μm. The aberration functions are scaled by 2π, and the average defocus has been subtracted. The arrows have been added for the sake of clarity; their direction is arbitrary from a physical point of view.

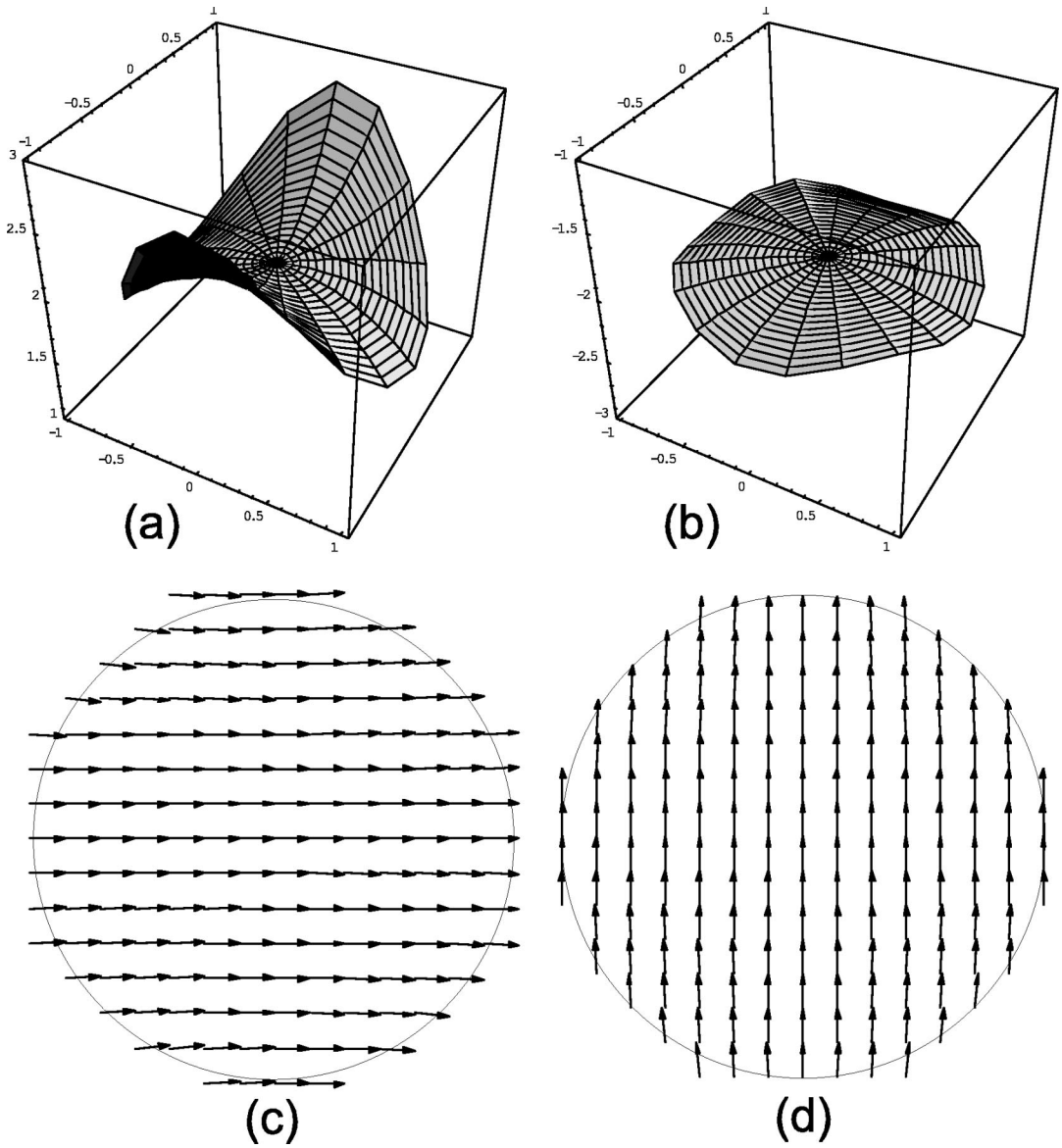

Fig. 5. Aberration functions of the (a) extraordinary and (b) ordinary modes, and polarization fields of the (c) extraordinary and (d) ordinary modes as a function of pupil coordinates for a uniaxially birefringent layer with optic axis perpendicular to the optical axis. The circle in the bottom panels indicates the pupil rim. We have taken $\Delta n_{\parallel} = -2\Delta n_{\perp} = 0.016$, $\bar{n} = 1.58$, NA $= 0.85$, $d = 100$ μm, and $\lambda = 0.405$ μm. The aberration functions are scaled by 2π, and the average defocus has been subtracted. The arrows have been added for the sake of clarity; their direction is arbitrary from a physical point of view.

$$\tan^2 \theta_c = \frac{2\Delta n_{\parallel}}{\Delta n_{\parallel} + 2\Delta n_{\perp}}. \tag{55}$$

For polar angles smaller than θ_c the aberration functions have a saddle shape of opposite sign (representing astigmatism); for polar angles larger than θ_c the aberration functions have a parabolic shape of opposite sign (representing defocus). As $\Delta n_{\parallel}/\Delta n_{\perp}$ is increased the zero-retardation points at θ_c move out of the pupil, giving two largely astigmatic aberration functions. When $\Delta n_{\perp}$ approaches zero one of the two aberration functions flattens out. The eigenpolarizations reflect the same crossover behavior. For polar angles smaller than θ_c the eigenpolarizations are close to the symmetry axes at angles γ and $\gamma + \pi/2$, similar to the case of lateral birefringence, whereas for polar angles larger than θ_c the eigenpolarizations are close to the radial and azimuthal directions, similar to the case of axial birefringence. Along the optical axes the eigenpolarizations are ill defined. When the eigenpolarizations are parallel transported over a loop around this singularity they experience a geometric phase π, i.e., they change sign.[33,34] Figure 6 shows the aberration functions and polarization fields for $\Delta n_{\perp} = 0.016$ and $\Delta n_{\parallel} = 0.002$ (and the same values for $\bar{n}$, NA, d, and λ as for the uniaxial birefringence cases). The differences between the part of the pupil close to the optical axis, which is similar to the lateral birefringence case, and the part of the pupil close to the rim, which is similar to the axial birefringence case, are as described above.

Stamnes and coworkers[24] have considered the limiting case of a small NA in some detail. When NA $\ll \bar{n} \sin \theta_c$ the intricate behavior of the eigenmodes close to the optic

axes does not play a role. The eigenpolarizations are then substantially uniformly linear across the pupil at angles γ and $\gamma + \pi/2$, and both eigenmodes are astigmatically aberrated. The astigmatic distances obtained from Eq. (43) in the limit of small NA are $d(\Delta n_{\parallel}/2 - \Delta n_{\perp})$ for the +mode and $d(\Delta n_{\parallel}/2 + \Delta n_{\perp})$ for the −mode. This is in agreement in the limit of small birefringence with the expressions $(n_1^2 - n_3^2)/n_1 n_3^2 (z_1 - z_0)/n^{(1)}$ and $(n_3^2 - n_2^2)/n_2 n_3^2 (z_1 - z_0)/n^{(1)}$ obtained in Ref. 24 [$n^{(1)}$ is the refractive index of the isotropic medium in front of the medium and $z_1 - z_0$ is the distance between the front surface and the focal point before inserting the medium into the converging beam of light, and $d = (z_1 - z_0)\bar{n}/n^{(1)}$].

B. Derivation of Aberration Functions and Eigenpolarization Vectors

In this subsection the expressions for $W_{\pm}$ and χ are formally derived. This subsection may be skipped by the less mathematically inclined readers.

The starting point is a formal plane-wave solution of Maxwell's equations in the biaxially birefringent medium. Consider a plane wave with wave vector $\mathbf{k}$ propagating in the medium. The components of $\mathbf{k}$ are given by

$$k_x = nk \sin\theta' \cos\phi, \tag{56}$$

$$k_y = nk \sin\theta' \sin\phi, \tag{57}$$

$$k_z = nk \cos\theta', \tag{58}$$

where n is the refractive index of the medium, to be determined later on. Orthogonal to $\mathbf{k}$ are polarization vectors $\hat{p}$ and $\hat{s}$:

$$\hat{p} = (\cos\theta' \cos\phi,\ \cos\theta' \sin\phi,\ -\sin\theta'), \tag{59}$$

$$\hat{s} = (-\sin\phi,\ \cos\phi,\ 0). \tag{60}$$

The magnetic field and induction can be eliminated from Maxwell's equations for a plane wave, giving the following equation for the electric field $\mathbf{E}$ and the dielectric displacement $\mathbf{D}$:

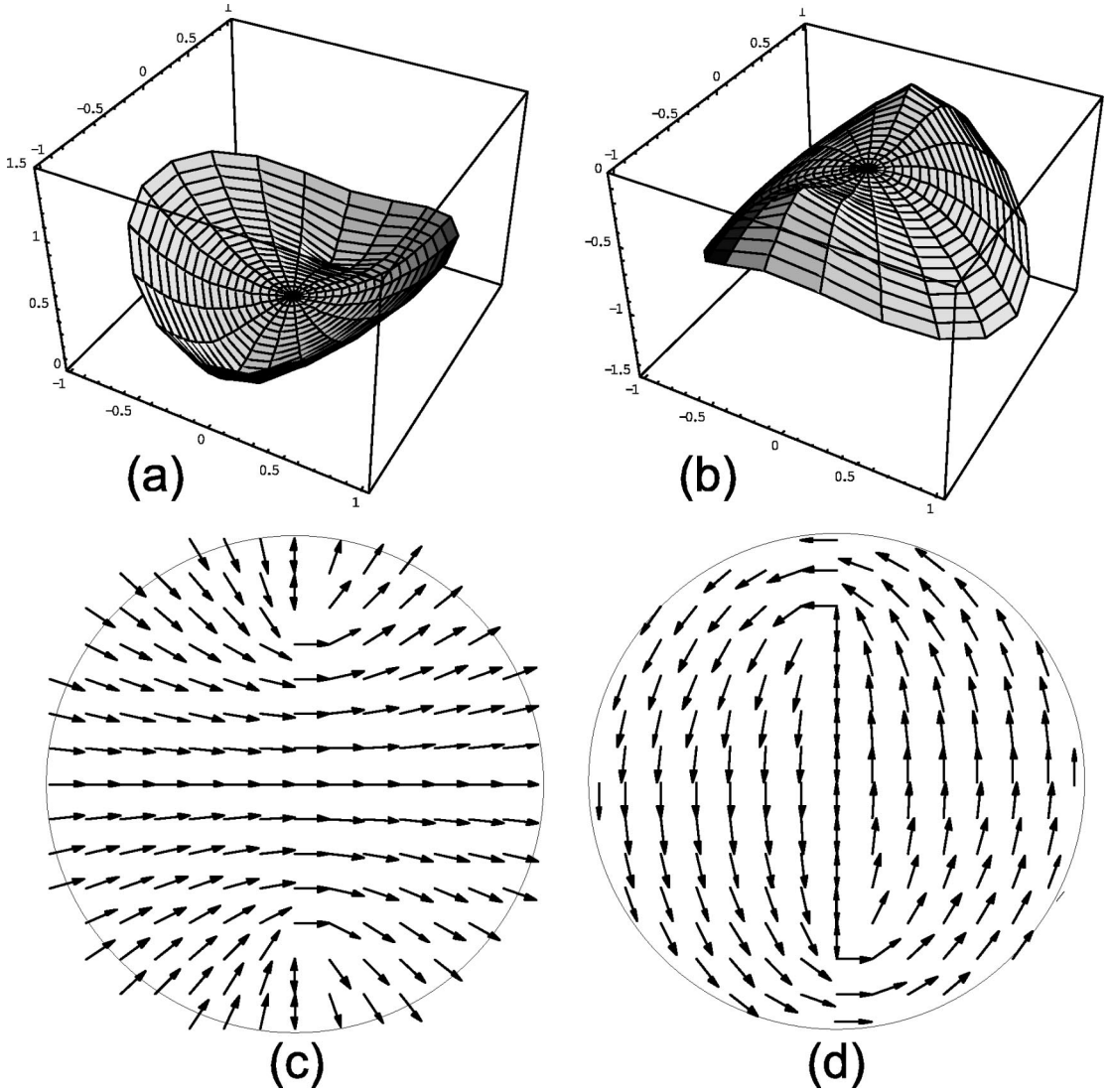

Fig. 6. Aberration functions of the (a) extraordinary and (b) ordinary modes and polarization fields of the (c) extraordinary and (d) ordinary modes as a function of pupil coordinates for a biaxially birefringent layer. The circle in (c) and (d) indicates the pupil rim. We have taken $\Delta n_{\perp} = 0.016$, $\Delta n_{\parallel} = 0.002$, $\bar{n} = 1.58$, NA = 0.85, $d = 100\ \mu$m, $\lambda = 0.4059\ \mu$m. The aberration functions are scaled by 2π, and the average defocus has been subtracted. The arrows have been added for the sake of clarity; their direction is arbitrary from a physical point of view. This is indicated by the opposing arrows on the line connecting the zero-retardation points.

$$\frac{1}{\varepsilon_0}\frac{\omega^2}{c^2}D_\alpha = [\mathbf{k}^2\delta_{\alpha\beta} - k_\alpha k_\beta]E_\beta. \tag{61}$$

Clearly, $\mathbf{D}$ is perpendicular to $\mathbf{k}$. As a consequence, D may be written as

$$D_\alpha = D_p p_\alpha + D_s s_\alpha. \tag{62}$$

The electric field may be eliminated by using the constitutive relation

$$D_\alpha = \varepsilon_0\varepsilon_{\alpha\beta}E_\beta, \tag{63}$$

with the dielectric tensor

$$\varepsilon_{\alpha\beta} = \begin{bmatrix} \cos\gamma & -\sin\gamma & 0 \\ \sin\gamma & \cos\gamma & 0 \\ 0 & 0 & 1 \end{bmatrix}\begin{bmatrix} {n_1}^2 & 0 & 0 \\ 0 & {n_2}^2 & 0 \\ 0 & 0 & {n_3}^2 \end{bmatrix} \times \begin{bmatrix} \cos\gamma & \sin\gamma & 0 \\ -\sin\gamma & \cos\gamma & 0 \\ 0 & 0 & 1 \end{bmatrix}, \tag{64}$$

giving

$$E_\alpha = \frac{1}{\varepsilon_0}(D_p\varepsilon^{-1}_{\alpha\beta}p_\beta + D_s\varepsilon^{-1}_{\alpha\beta}s_\beta). \tag{65}$$

Substitution results in the following equations for D_p and D_s:

$$\begin{bmatrix} M_{11} - 1/n^2 & M_{12} \\ M_{21} & M_{22} - 1/n^2 \end{bmatrix}\begin{bmatrix} D_p \\ D_s \end{bmatrix} = \begin{bmatrix} 0 \\ 0 \end{bmatrix}, \tag{66}$$

with the matrix elements

$$M_{11} = p_\alpha\varepsilon^{-1}_{\alpha\beta}p_\beta = \frac{\cos^2\theta'\cos^2(\gamma-\phi)}{{n_1}^2} + \frac{\cos^2\theta'\sin^2(\gamma-\phi)}{{n_2}^2} + \frac{\sin^2\theta'}{{n_3}^2}, \tag{67}$$

$$M_{12} = p_\alpha\varepsilon^{-1}_{\alpha\beta}s_\beta = -\left(\frac{1}{{n_2}^2} - \frac{1}{{n_1}^2}\right)\cos\theta' \times \sin(\gamma-\phi)\cos(\gamma-\phi), \tag{68}$$

$$M_{21} = s_\alpha\varepsilon^{-1}_{\alpha\beta}p_\beta = -\left(\frac{1}{{n_2}^2} - \frac{1}{{n_1}^2}\right)\cos\theta' \times \sin(\gamma-\phi)\cos(\gamma-\phi), \tag{69}$$

$$M_{22} = s_\alpha\varepsilon^{-1}_{\alpha\beta}s_\beta = \frac{\sin^2(\gamma-\phi)}{{n_1}^2} + \frac{\cos^2(\gamma-\phi)}{{n_2}^2}. \tag{70}$$

Nontrivial solutions of the characteristic equation Eq. (66) are found when the determinant of this symmetric 2×2 matrix equals zero, or

$$[M_{11} - 1/n^2][M_{22} - 1/n^2] - {M_{12}}^2 = 0. \tag{71}$$

The two solutions corresponding to the two eigenmodes are

$$\frac{1}{{n_\pm}^2} = \frac{M_{11}+M_{22}}{2} \mp \left[\left(\frac{M_{11}-M_{22}}{2}\right)^2 + {M_{12}}^2\right]^{1/2}. \tag{72}$$

The eigenvectors $\mathbf{D}_\pm$ of the two modes are orthogonal because of the symmetry of the 2×2 matrix in Eq. (66). It follows that the eigenvectors can be expressed in the following form,

$$D_{+\alpha} = \varepsilon_0 A_+ {n_+}^2[\cos(\chi-\phi)p_\alpha + \sin(\chi-\phi)s_\alpha], \tag{73}$$

$$D_{-\alpha} = \varepsilon_0 A_- {n_-}^2[-\sin(\chi-\phi)p_\alpha + \cos(\chi-\phi)s_\alpha], \tag{74}$$

where A_+ and A_- are constants, to be fixed by the boundary conditions, and where χ is an angle to be determined from the characteristic equation (66). The corresponding electric fields are

$$E_{+\alpha} = A_+{n_+}^2[\cos(\chi-\phi)\varepsilon^{-1}_{\alpha\beta}p_\beta + \sin(\chi-\phi)\varepsilon^{-1}_{\alpha\beta}s_\beta] = A_+[\cos(\chi-\phi)p_\alpha + \sin(\chi-\phi)s_\alpha + e_+k_\alpha], \tag{75}$$

$$E_{-\alpha} = A_-{n_-}^2[-\sin(\chi-\phi)\varepsilon^{-1}_{\alpha\beta}p_\beta + \cos(\chi-\phi)\varepsilon^{-1}_{\alpha\beta}s_\beta] = A_-[-\sin(\chi-\phi)p_\alpha + \cos(\chi-\phi)s_\alpha + e_-k_\alpha], \tag{76}$$

where e_+ and e_- are proportional to the birefringence parameters and are therefore small compared to one. These small electric field components are responsible for the rays' not being perpendicular to the wave fronts, i.e., for the different refraction of the two eigenmodes. By using the expressions for the refractive indices of the eigenmodes the angle χ turns out to be given by

$$\cos(2\chi - 2\phi) = -\frac{(M_{11}-M_{22})/2}{\{[(M_{11}-M_{22})/2]^2 + {M_{12}}^2\}^{1/2}}, \tag{77}$$

$$\sin(2\chi - 2\phi) = -\frac{M_{12}}{\{[(M_{11}-M_{22})/2]^2 + {M_{12}}^2\}^{1/2}}. \tag{78}$$

The angle ϕ is present in these equations for future convenience. This completes the general solution.

The biaxially birefringent medium has an interface with air perpendicular to the z axis. A plane wave propagating in air along

$$\mathbf{k}_{\text{air}} = k(\sin\theta\cos\phi,\ \sin\theta\sin\phi,\ \cos\theta), \tag{79}$$

will be refracted into two waves corresponding to the two modes with polar angles $\theta'_\pm$ given by Snell's law:

$$\sin\theta = n_\pm\sin\theta'_\pm. \tag{80}$$

As the refractive indices $n_\pm$ depend on $\theta'_\pm$ this is an equation for this angle. In general, angles θ'_+ and θ'_- are different. The resulting wave vectors of the two modes can be expressed as

$$\mathbf{k}_\pm = k(\sin\theta\cos\phi,\ \sin\theta\sin\phi,\ ({n_\pm}^2 - \sin^2\theta)^{1/2}), \tag{81}$$

where Snell's law and $|\mathbf{k}_\pm|^2 = k^2{n_\pm}^2$ are used.

The mode amplitudes A_+ and A_- can be expressed in terms of the p and s amplitudes of the isotropic medium in front of the biaxially birefringent medium as

$$\begin{bmatrix} A_+ \\ A_- \end{bmatrix} = \begin{bmatrix} T_{+p} & T_{+s} \\ T_{-p} & T_{-s} \end{bmatrix} \begin{bmatrix} A_p \\ A_s \end{bmatrix}, \tag{82}$$

where the numbers $T_{\pm p}$ and $T_{\pm s}$ describe the interface coupling. These numbers must be solved from the boundary conditions for the electromagnetic field at the interface.

To this point no approximations have been made. From here on the small-birefringence approximation will be used. The matrix elements M_{jk} may be rewritten in terms of the birefringence parameters as

$$\frac{M_{11}+M_{22}}{2} = \frac{1}{\bar{n}^2} - \frac{1}{\bar{n}^3}\left[\Delta n_\perp \sin^2\theta'_\pm - \frac{1}{2}\Delta n_\parallel \sin^2\theta'_\pm \cos(2\gamma - 2\phi)\right], \tag{83}$$

$$\frac{M_{11}-M_{22}}{2} = -\frac{1}{\bar{n}^3}\left[\Delta n_\perp \sin^2\theta'_\pm + \frac{1}{2}\Delta n_\parallel (1+\cos^2\theta'_\pm)\cos(2\gamma - 2\phi)\right], \tag{84}$$

$$M_{12} = -\frac{1}{\bar{n}^3}[\Delta n_\parallel \cos\theta'_\pm \sin(2\gamma - 2\phi)]. \tag{85}$$

The angles $\theta'_\pm$ can be taken equal to the angle of refraction in the isotropic limit of zero birefringence, i.e., $\sin\theta'_\pm = \sin\theta' = \sin\theta/\bar{n}$. Equations (44) and (45) for the angle χ now follow directly. Also, the electric field may be taken in the plane spanned by the polarization vectors $\hat{p}$ and $\hat{s}$, as the component along $\hat{k}$ is proportional to the small-birefringence parameters. The resulting polarization vectors of the + and − modes make an angle $\chi - \phi$ with $\hat{p}$ and $\hat{s}$, respectively.

The refractive indices of the eigenmodes are given by

$$\frac{1}{n_\pm^2} = \frac{1}{\bar{n}^2} - \frac{a \pm (b^2+c^2)^{1/2}}{\bar{n}^3}, \tag{86}$$

where the parameters a, b, and c, defined in Eqs. (46), (47), and (48), are proportional to the birefringence parameters. In the small-birefingence limit the refractive indices of the two eigenmodes then follow as

$$n_\pm = \bar{n} + a \pm (b^2+c^2)^{1/2}, \tag{87}$$

and the z component of the wave vector is

$$k_{z\pm} = k(n_\pm^2 - \sin^2\theta)^{1/2} = k\bar{n}\cos\theta' + \frac{k}{2\cos\theta'}[a \mp (b^2+c^2)^{1/2}]. \tag{88}$$

In the limit of zero birefringence the z component is simply $k\bar{n}\cos\theta'$. The lateral wave vector components are then still the same as they are fixed by Snell's law for refraction at the isotropic–birefringent interface. Consequently, the phase difference between the nonzero birefringence case and the zero birefringence case is

$$W_\pm = (k_{z\pm} - k\bar{n}\cos\theta')d, \tag{89}$$

which gives the aberration functions of the two eigenmodes according to Eq. (43).

The mode coupling at the interface can be simplified as well. Effects of the small-birefringence parameters on the interface matrix elements are only small amplitude effects and can be safely neglected. The interface can thus be described by the Fresnel coefficients t_p and t_s of the interface between air and an isotropic medium with refractive index $\bar{n}$. This is entirely similar to the approach described in the text of Yeh[25] for uniaxial media. From Eqs. (75) and (76) the following relations between the mode amplitudes and the entrance pupil amplitudes A_1 and A_2 can now be obtained:

$$\cos(\chi-\phi)A_+ - \sin(\chi-\phi)A_- = t_p(\cos\phi A_1 + \sin\phi A_2), \tag{90}$$

$$-\sin(\chi-\phi)A_+ + \cos(\chi-\phi)A_- = t_s(-\sin\phi A_1 + \cos\phi A_2), \tag{91}$$

leading to

$$\begin{bmatrix} A_+ \\ A_- \end{bmatrix} = R(-\chi) J_{\text{en}} \begin{bmatrix} A_1 \\ A_2 \end{bmatrix}, \tag{92}$$

where J_{en} is the interface Jones matrix as given in Eq. (16). The overall Jones matrix for focusing into the biaxially birefringent medium then follows as $J_{\text{bir}}J_{\text{en}}$, where J_{bir} is the birefringence Jones matrix as defined in Eq. (42).

4. NUMERICAL RESULTS

A. Multipole Expansion of the Diffraction Integrals

The diffraction integrals are evaluated in terms of a multipole expansion.[35] The method used is a variation of the method proposed by Sheppard and Török.[11] The diffraction integrals can be cast in the form

$$F_{\alpha j}(\mathbf{r}_p) = \frac{1}{4\pi}\int_0^\beta d\theta \sin\theta \int_0^{2\pi} d\phi V_{\alpha j}(\theta,\phi)\exp(i\mathbf{k}\cdot\mathbf{r}_p), \tag{93}$$

where

$$V_{\alpha j}(\theta,\phi) = \frac{4\cos\theta}{\sin^2\beta}\sum_{s=1,2}\hat{v}_{\alpha s}J_{sj}, \tag{94}$$

is the pupil function, and where the phase may be written as

$$\mathbf{k}\cdot\mathbf{r}_p = nkr_p\cos\zeta = nkr_p[\cos\theta\cos\theta_p + \sin\theta\sin\theta_p\cos(\phi-\phi_p)], \tag{95}$$

where the parametrization of $\mathbf{r}_p$ in spherical coordinates is used. Using Bauer's formula the phase term may be rewritten as

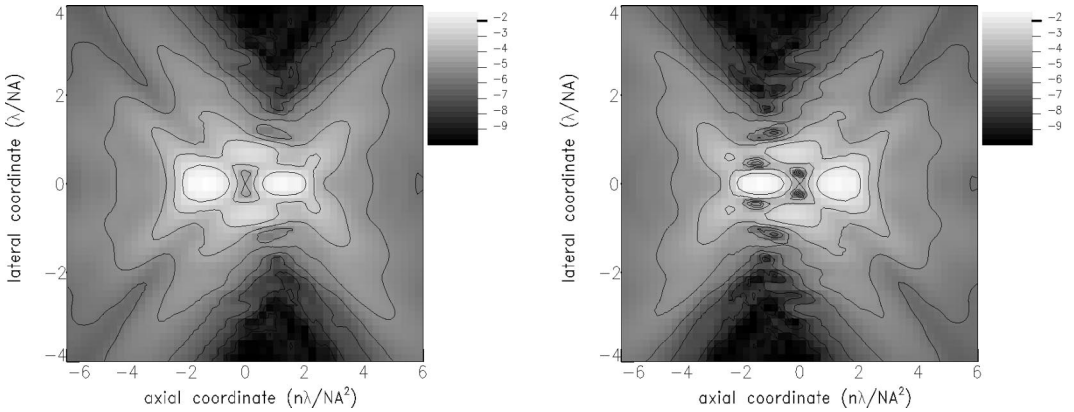

Fig. 7. Intensity distribution in the meridional planes parallel (left) and perpendicular (right) to the linear entrance polarization for the case of axial birefringence. Parameters used are $\Delta n_\perp = 0.016$, $\bar{n} = 1.58$, NA = 0.85, $d = 100\ \mu$m, and $\lambda = 0.405\ \mu$m. The intensity distribution is plotted logarithmically to show relatively fine details.

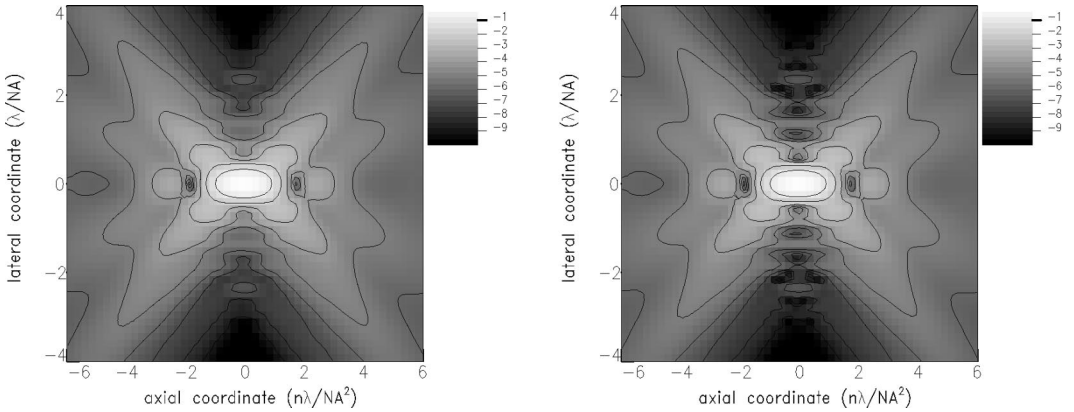

Fig. 8. Intensity distribution in the meridional planes parallel (left) and perpendicular (right) to the linear entrance polarization for the case of lateral birefringence with the entrance polarization perpendicular to the principal axis (ordinary mode). Parameters used are $\Delta n_\parallel = 2\Delta n_\perp = 0.016$, $\bar{n} = 1.58$, NA = 0.85, $d = 100\ \mu$m, $\lambda = 0.405\ \mu$m. The intensity distribution is plotted logarithmically to show relatively fine details.

$$\exp(inkr_p \cos\zeta) = \sum_{l=0}^{\infty} i^l (2l+1) j_l(nkr_p) P_l(\cos\zeta), \tag{96}$$

with $j_l(x)$ the spherical Bessel function of order l and $P_l(x)$ the Legendre polynomial of order l. This Legendre polynomial may be rewritten in terms of spherical harmonics by using the addition theorem,

$$P_l(\cos\zeta) = \frac{4\pi}{2l+1} \sum_{m=-l}^{l} Y^*_{lm}(\theta, \phi) Y_{lm}(\theta_p, \phi_p), \tag{97}$$

leading to

$$\exp(i\mathbf{k}\cdot\mathbf{r}_p) = 4\pi \sum_{l=0}^{\infty} \sum_{m=-l}^{l} i^l Y^*_{lm}(\theta, \phi) Y_{lm}(\theta_p, \phi_p) j_l(nkr_p). \tag{98}$$

Substitution in the diffraction integral gives the final result,

$$F_{\alpha j}(\mathbf{r}_p) = \sum_{l=0}^{\infty} \sum_{m=-l}^{l} F^{lm}_{\alpha j} Y_{lm}(\theta_p, \phi_p) j_l(nkr_p), \tag{99}$$

with the coefficients

$$F^{lm}_{\alpha j} = (-i)^l \int_0^{\beta} d\theta \sin\theta \int_0^{2\pi} d\phi Y^*_{lm}(\theta, \phi) V_{\alpha j}(\theta, \phi). \tag{100}$$

Clearly, we have expanded the field close to focus in terms of partial waves or multipoles, which are elementary solutions of the scalar wave equation. As each electric field component satisfies the wave equation it follows directly that such an expansion is possible. The surprising advantage of the Debye approach is that the coefficients of the expansion $F^{lm}_{\alpha j}$ can be easily expressed in terms of the pupil function. This approach is similar in spirit to that of Kant,[9,10] later followed in Ref. 14, the difference being that Kant's expansion is based on the Gegenbauer polynomials instead of the spherical harmonics of the present method. The use of the multipole expansion was first proposed by Sheppard and Török.[11] In the simple case without aberrations or birefringence they even showed that the three components of the full vectorial field can be derived from a single set of multipole coefficients. Finally, it is mentioned that the multipole expansion of the image field of Eqs. (99) and (100) can also be derived from the eigenfunction expansion of the Green's function,[35] the far-field behavior of spherical Hankel functions, and the (second) Rayleigh–Sommerfeld form of the diffraction integral.

The multipole expansion works best for moderate to high NA values. Then the spatial extent of the focal spot is relatively small, meaning that the argument of the spherical Bessel function is relatively small. For small arguments the terms in the series decrease rapidly and the cutoff order $l_{\max}$ may be taken to be relatively low. For small NA, large birefringence, large aberrations, or far from focus, more terms in the expansion are needed to produce accurate results. The method is implemented as follows. First the pupil function is sampled, typically 16 azimuthal values and 129 radial values. The fast-Fourier-transform (FFT) method is applied to the azimuthal dependence and Romberg integration to the radial dependence.[36] For NA = 0.85 the cutoff at $l = 32$ and $m = 8$ gives accurate results. Calculating the expansion coefficients and the image field in ≈4000 points takes ≈1 s on present-day workstations.

A different eigenfunction method has recently been proposed by Janssen,[37] and by Braat, Dirksen, and Janssen.[38] Their eigenfunctions can be expressed as a fast-converging Taylor series in a defocus parameter of which the coefficients can be analytically expressed in terms of Bessel functions of integer order. The main advantage of eigenfunction expansions compared with brute force, FFT methods is that the same expansion coefficients can be used for all values of the axial position–defocus value. The FFT method requires a new calculation for each axial position–defocus value. On the other hand, efficient ways to evaluate FFTs are available in the literature.[39] It is an open question which method is the most efficient one for computing diffraction integrals.

B. Isophotes

Figure 7 shows contour plots of the intensity in the meridional planes parallel and perpendicular to the linear entrance polarization for focusing by an aplanatic lens into an axially birefringent layer with $\Delta n_\perp = 0.016$, $d = 100$ μm, $\lambda = 0.405$ μm, and NA = 0.85. These parameters correspond to the aberration functions and polarization fields of Fig. 4. The lines of constant intensity are called isophotes. The plots clearly show the two focal spots, corresponding to the ordinary and extraordinary modes, with different defocus. The uniform linear entrance polarization couples to both eigenmodes, as the eigenpolarizations are radially and azimuthally polarized. The entrance polarization couples differently to the eigenmodes in the planes parallel and perpendicular to the entrance polarization, leading to the asymmetry between the two focal spots in each meridional plane and to the asymmetry between the two meridional planes. Another consequence is the appearance of a secondary focal structure, namely, the ring in the original focal plane.

Figures 8 and 9 show the same plots for a laterally birefringent layer with $\Delta n_\parallel = 2\Delta n_\perp = 0.016$ for the linear entrance polarization perpendicular (ordinary mode) to the principal axis and parallel (extraordinary mode) to the principal axis. These parameters correspond to the aberration functions and polarization fields of Fig. 5. The ordinary mode is hardly affected by the birefringence, whereas the extraordinary mode is significantly aberrated by astigmatism, as can be clearly seen from the two focal "lines" that are orthogonal. When the entrance polarization is such that both modes are excited (e.g., for a circular polarization) the intensity distribution in the focal region of both modes becomes mixed.

Figure 10 shows intensity contour plots for a biaxial layer with $\Delta n_\parallel = 0.002$ and $\Delta n_\perp = 0.016$ for linear entrance polarizations along the x axis and along the y axis. The birefringence parameters correspond to the aberration functions and polarization fields of Fig. 6. Both entrance polarizations show that one of the two axially displaced focal spots of the axially birefringent case has become slightly astigmatic, whereas the other mixes with the secondary focal ring in three distinct parts. When the ratio $\Delta n_\parallel/\Delta n_\perp$ increases these structures reorganize into a hardly aberrated ordinary focal spot and an astig-

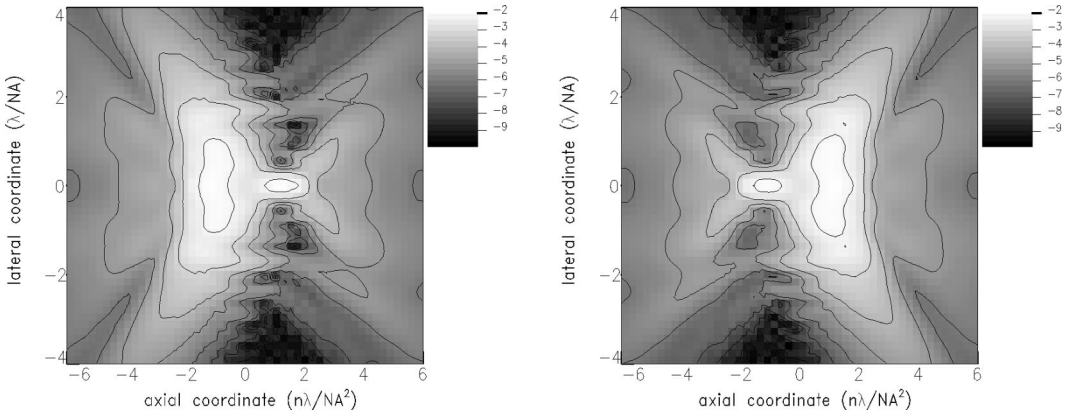

Fig. 9. Intensity distribution in the meridional planes parallel (left) and perpendicular (right) to the linear entrance polarization for the case of lateral birefringence with the entrance polarization parallel to the principal axis (extraordinary mode). Parameters used are $\Delta n_\parallel = 2\Delta n_\perp = 0.016$, $\bar{n} = 1.58$, NA = 0.85, $d = 100$ μm, and $\lambda = 0.405$ μm. The intensity distribution is plotted logarithmically to show relatively fine details.

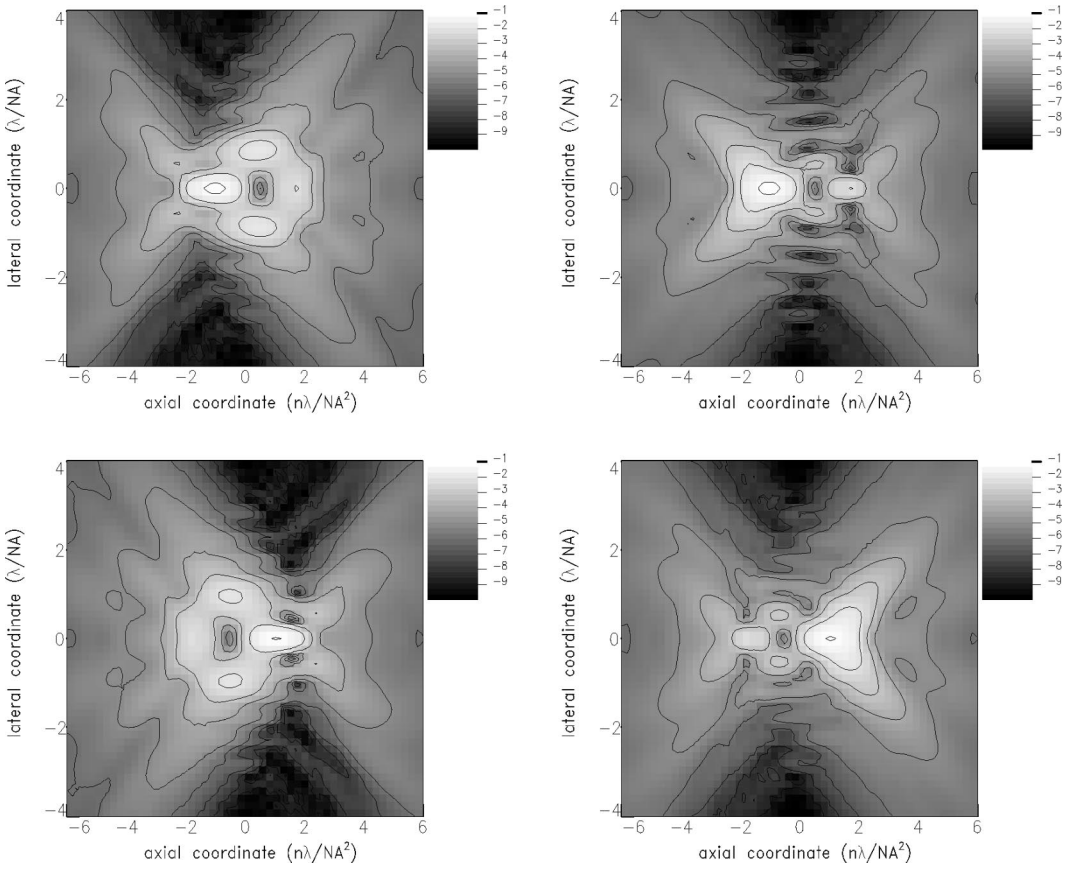

Fig. 10. Intensity distribution in the meridional xz (left) and yz (right) planes for a linear entrance polarization along the x axis (top) and along the y axis (bottom) for the case of biaxial birefringence with $\Delta n_{\perp} = 0.016$, $\Delta n_{\parallel} = 0.002$ (so $n_3 > n_1 > n_2$), $\gamma = 0$, $\bar{n} = 1.58$, NA = 0.85, $d = 100$ μm, and $\lambda = 0.405$ μm. The intensity distribution is plotted logarithmically to show relatively fine details.

matically aberrated extraordinary focal spot. This reorganization is most likely accompanied by creation and annihilation of singular structures of the kinds described in Ref. 40. This subject is not considered further here, but would certainly be of interest for a separate study.

5. SUMMARY AND CONCLUSION

The influence of focusing into a biaxially birefringent layer on the distribution of light close to focus is investigated by means of vectorial diffraction theory. The diffraction integrals are evaluated within the framework of the Debye approach and for small birefringence values. The field close to focus is the superposition of the field of the two polarization eigenmodes of the birefringent layer. In the limiting case of uniaxial birefringence with principal axis parallel to the optical axis, the most important effect is the relative defocus of the two polarization eigenmodes; when the principal axis is perpendicular to the optical axis the dominant effect is astigmatism in the extraordinary polarization eigenmode. For the biaxial case a crossover between the two cases occurs, as a result of which, for small angles of incidence, both modes are astigmatic, while for large angles of incidence both modes are relatively defocused. For the intermediate case the behavior is determined by the mode structure close to the optic axes of the biaxial medium.

The resulting blurring of the focal spot can be described by the deviation of the Strehl ratio from the ideal value of 1. An analytical calculation of the Strehl ratio based on a generalization of the ordinary scalar aberration theory is presented in a companion paper.

ACKNOWLEDGMENTS

Jean Schleipen and Paul Urbach are thanked for a critical reading of the manuscript.

Sjoerd Stallinga can be reached by e-mail at sjoerd.stallinga@philips.com.

REFERENCES

1. S. Stallinga, "Axial birefringence in high-NA optical systems and the light distribution close to focus," J. Opt. Soc. Am. A **18**, 2846–2858 (2001).
2. E. Wolf, "Electromagnetic diffraction in optical systems. I. An integral representation of the image field," Proc. R. Soc. London, Ser. A **253**, 349–357 (1959).
3. B. Richards and E. Wolf, "Electromagnetic diffraction in optical systems. II. Structure if the image field in an aplanatic system," Proc. R. Soc. London Ser. A **253**, 358–379 (1959).
4. A. Boivin and E. Wolf, "Electromagnetic field in the neighborhood of the focus of a coherent beam," Phys. Rev. B **138**, 1561–1565 (1965).
5. A. Boivin, J. Dow, and E. Wolf, "Energy flow in the neigh-

bourhood of the focus of a coherent beam," J. Opt. Soc. Am. **57**, 1171–1175 (1967).
6. M. Mansuripur, "Distribution of light at and near the focus of high-numerical-aperture objectives," J. Opt. Soc. Am. A **3**, 2086–2093 (1986).
7. M. Mansuripur, "Certain computational aspects of vector diffraction problems," J. Opt. Soc. Am. A **6**, 786–805 (1989).
8. M. Mansuripur, "Distribution of light at and near the focus of high-numerical-aperture objectives: erratum; Certain computational aspects of vector diffraction problems: erratum," J. Opt. Soc. Am. A **10**, 382–383 (1993).
9. R. Kant, "An analytical solution of vector diffraction for focusing optical systems," J. Mod. Opt. **40**, 337–347 (1993).
10. R. Kant, "An analytical solution of vector diffraction for focusing optical systems with Seidel aberrations. I. Spherical aberration, curvature of field, and distortion," J. Mod. Opt. **40**, 2293–2310 (1993).
11. C. J. R. Sheppard and P. Török, "Efficient calculation of electromagnetic diffraction in optical systems using a multipole expansion," J. Mod. Opt. **44**, 803–818 (1997).
12. H. Ling and S.-W. Lee, "Focusing of electromagnetic waves through a dielectric interface," J. Opt. Soc. Am. A **1**, 965–973 (1984).
13. P. Török, P. Varga, Z. Laczik, and G. R. Booker, "Electromagnetic diffraction of light focused through a planar interface between materials of mismatched refractive indices: an integral representation," J. Opt. Soc. Am. A **12**, 325–332 (1995).
14. P. Török, P. Varga, and G. R. Booker, "Electromagnetic diffraction of light focused through a planar interface between materials of mismatched refractive indices: structure of the electromagnetic field. I," J. Opt. Soc. Am. A **12**, 2136–2144 (1995).
15. P. Török, P. Varga, and G. Németh, "Analytical solution of the diffraction integrals and interpretation of wave-front distortion when light is focused through a planar interface between materials of mismatched refractive indices," J. Opt. Soc. Am. A **12**, 2660–2671 (1995).
16. S. H. Wiersma and T. D. Visser, "Defocusing of a converging electromagnetic wave by a plane dielectric interface," J. Opt. Soc. Am. A **13**, 320–325 (1996).
17. S. H. Wiersma, P. Török, T. D. Visser, and P. Varga, "Comparison of different theories for focusing through a plane interface," J. Opt. Soc. Am. A **14**, 1482–1490 (1997).
18. V. Dhayalan and J. J. Stamnes, "Focusing of electromagnetic waves into a dielectric slab: I. Exact and asymptotic results," Pure Appl. Opt. **6**, 33–52 (1997).
19. D. G. Flagello, T. Milster, and A. E. Rosenbluth, "Theory of high-NA imaging in homogeneous thin films," J. Opt. Soc. Am. A **13**, 53–64 (1996).
20. J. J. Stamnes and D. Jiang, "Focusing of electromagnetic waves into a uniaxial crystal," Opt. Commun. **150**, 251–262 (1998).
21. D. Jiang and J. J. Stamnes, "Numerical and asymptotic results for focusing of two-dimensional waves in uniaxial crystals," Opt. Commun. **163**, 55–71 (1999).
22. D. Jiang and J. J. Stamnes, "Numerical and experimental results for focusing of two-dimensional electromagnetic waves into uniaxial crystals," Opt. Commun. **174**, 321–334 (2000).
23. J. J. Stamnes and G. Sithambaranathan, "Reflection and refraction of an arbitrary electromagnetic wave at a plane interface separating an isotropic and a biaxial medium," J. Opt. Soc. Am. A **18**, 3119–3129 (2001).
24. J. J. Stamnes, G. Sithambaranathan, M. Jain, J. K. Lotsberg, and V. Dhayalan, "Focusing of electromagnetic waves into a biaxial crystal," Opt. Commun. **226**, 107–123 (2003).
25. P. Yeh, *Optical Waves in Layered Media* (Wiley, New York, 1988).
26. J. J. Stamnes, *Waves in Focal Regions* (Hilger, Bristol, UK, 1986).
27. J. J. Stamnes, ed., *Electromagnetic Fields in the Focal Region*, SPIE Milestone Volume 168 (SPIE Optical Engineering Press, Bellingham, Wash., 2001).
28. M. K. Dekker, N. Pfeffer, M. Kuijper, W. M. Coene, E. R. Meinders, and H. J. Borg, "Blue phase-change recording at high data densities and data rates," in *Optical Data Storage 2000*, D. G. Stinson and R. Katayama, eds., Proc. SPIE **4090**, 28–35 (2000).
29. I. Ichimura, S. Masuhara, J. Nakano, Y. Kasami, K. Yasuda, O. Kawakubo, and K. Osato, "On-groove phase-change optical recording for a capacity of 25 Gbytes," in *Optical Data Storage 2001*, T. Hurst and S. Kobayashi, eds., Proc. SPIE **4342**, 168–177 (2001).
30. M. Kuijper, I. P. Ubbens, L. Spruijt, J. M. ter Meulen, and K. Schep, "Groove-only recording under DVR conditions," in *Optical Data Storage 2001*, T. Hurst and S. Kobayashi, eds., Proc. SPIE **4342**, 178–185 (2001).
31. M. Born and E. Wolf, *Principles of Optics*, 6th ed. (Cambridge U. Press, Cambridge, UK, 1980).
32. T. D. Goodman and M. Mansuripur, "Subtle effects of the substrate in optical disk data storage systems," Appl. Opt. **35**, 6747–6753 (1996).
33. R. Bhandari, "Polarization of light and topological phases," Phys. Rep. **281**, 1–64 (1997).
34. M. Berry, R. Bhandari, and S. Klein, "Black plastic sandwiches demonstrating biaxial optical anisotropy," Eur. J. Phys. **20**, 1–14 (1999).
35. J. D. Jackson, *Classical Electrodynamics* (Wiley, New York, 1975).
36. W. H. Press, S. A. Teukolsky, W. T. Vetterling, and B. P. Flannery, *Numerical Recipes in Fortran 77: The Art of Scientific Computing*, 2nd ed. (Cambridge U. Press, Cambridge, UK, 1992).
37. A. J. E. M. Janssen, "Extended Nijboer-Zernike approach for the computation of optical point-spread functions," J. Opt. Soc. Am. A **19**, 849–857 (2002).
38. J. J. M. Braat, P. Dirksen, and A. J. E. M. Janssen, "Assessment of an extended Nijboer-Zernike approach for the computation of optical point-spread functions," J. Opt. Soc. Am. A **19**, 858–870 (2002).
39. J. L. Bakx, "Efficient computation of optical disk readout by use of the chirp z transform," Appl. Opt. **41**, 4897–4903 (2002).
40. J. F. Nye, *Natural Focusing and Fine Structure of Light* (Institute of Physics, Bristol, UK, 1999).